blood®
Regular Article

IMMUNOBIOLOGY AND IMMUNOTHERAPY

SASH3 variants cause a novel form of X-linked combined immunodeficiency with immune dysregulation

Ottavia M. Delmonte,[1] Jenna R. E. Bergerson,[1] Tomoki Kawai,[1] Hye Sun Kuehn,[2] David H. McDermott,[3] Irene Cortese,[4] Michael T. Zimmermann,[5,6] A. Kerry Dobbs,[1] Marita Bosticardo,[1] Danielle Fink,[7] Shamik Majumdar,[3] Boaz Palterer,[8] Francesca Pala,[1] Nikita R. Dsouza,[5] Marie Pouzolles,[9] Naomi Taylor,[9,10] Katherine R. Calvo,[11] Stephen R. Daley,[12] Daniel Velez,[3] Anahita Agharahimi,[1] Katherine Myint-Hpu,[1] Lesia K. Dropulic,[13] Jonathan J. Lyons,[14] Steven M. Holland,[1] Alexandra F. Freeman,[1] Rajarshi Ghosh,[1] Morgan B. Similuk,[1] Julie E. Niemela,[2] Jennifer Stoddard,[2] Douglas B. Kuhns,[7] Raul Urrutia,[5,15] Sergio D. Rosenzweig,[2] Magdalena A. Walkiewicz,[1] Philip M. Murphy,[3] and Luigi D. Notarangelo[1]

[1]Laboratory of Clinical Immunology and Microbiology, Division of Intramural Research, National Institute of Allergy and Infectious Diseases, National Institutes of Health, Bethesda, MD; [2]Department of Laboratory Medicine, Clinical Center, National Institutes of Health, Bethesda, MD; [3]Molecular Signaling Section, Laboratory of Molecular Immunology, Division of Intramural Research, National Institute of Allergy and Infectious Diseases, National Institutes of Health, Bethesda, MD; [4]Neuroimmunology Clinic, Division of Neuroimmunology and Neurovirology, National Institute of Neurological Disorders and Stroke, National Institutes of Health, Bethesda, MD; [5]Division of Research, Genomics Sciences & Precision Medicine Center, Milwaukee, WI; [6]Clinical and Translational Sciences Institute, Medical College of Wisconsin, Milwaukee, WI; [7]Applied/Developmental Research Directorate, Leidos Biomedical Research, Inc, Frederick National Laboratory for Cancer Research, Frederick, MD; [8]Department of Experimental and Clinical Medicine, University of Florence, Florence, Italy; [9]Pediatric Oncology Branch, National Cancer Institute, National Institutes of Health, Bethesda, MD; [10]Institut de Genetique Moleculaire de Montpellier, Centre National de la Recherche Scientifique Unité Mixte de Recherche (UMR) 5535, Universite de Montpellier, Montpellier, France; [11]Hematology Section, Department of Laboratory Medicine, Clinical Center, National Institutes of Health, Bethesda, MD; [12]Centre for Immunology and Infection Control, School of Biomedical Sciences, Faculty of Health, Queensland University of Technology, Brisbane, QLD, Australia; [13]Laboratory of Infectious Disease and [14]Division of Intramural Research, Laboratory of Allergic Diseases, Division of Intramural Research, National Institute of Allergy and Infectious Diseases, National Institutes of Health, Bethesda, MD and;[15]Department of Surgery, Medical College of Wisconsin, Milwaukee, WI

KEY POINTS

- **SASH3 is an adaptor protein expressed mainly in lymphocytes that is important for T-cell proliferation and activation and cell survival.**
- **Hemizygous loss-of-function variants in *SASH3* result in combined immunodeficiency with immune dysregulation.**

Sterile alpha motif (SAM) and Src homology-3 (SH3) domain-containing 3 (SASH3), also called SH3-containing lymphocyte protein (SLY1), is a putative adaptor protein that is postulated to play an important role in the organization of signaling complexes and propagation of signal transduction cascades in lymphocytes. The *SASH3* gene is located on the X-chromosome. Here, we identified 3 novel *SASH3* deleterious variants in 4 unrelated male patients with a history of combined immunodeficiency and immune dysregulation that manifested as recurrent sinopulmonary, cutaneous, and mucosal infections and refractory autoimmune cytopenias. Patients exhibited $CD4^+$ T-cell lymphopenia, decreased T-cell proliferation, cell cycle progression, and increased T-cell apoptosis in response to mitogens. In vitro T-cell differentiation of $CD34^+$ cells and molecular signatures of rearrangements at the T-cell receptor α (*TRA*) locus were indicative of impaired thymocyte survival. These patients also manifested neutropenia and B-cell and natural killer (NK)-cell lymphopenia. Lentivirus-mediated transfer of the *SASH3* complementary DNA–corrected protein expression, in vitro proliferation, and signaling in SASH3-deficient Jurkat and patient-derived T cells. These findings define a new type of X-linked combined immunodeficiency in humans that recapitulates many of the abnormalities reported in mice with *Sly1*$^{-/-}$ and *Sly1*$^{\Delta/\Delta}$ mutations, highlighting an important role of SASH3 in human lymphocyte function and survival.

Introduction

Antigen receptor engagement on lymphocytes allows for initiation of signal transduction pathways that ultimately guide the cellular immune response.[1] Genetic defects associated with impaired antigen receptor signaling are a cause of combined immunodeficiency (CID) in humans, with increased susceptibility to severe infections, autoimmunity, and malignancies.[2,3]

Adaptor proteins play an important role in the propagation of signal transduction cascades. Through recognition of protein-protein interaction domains, adaptor molecules function as intracellular scaffolds around which signaling complexes are organized. SASH3 (sterile alpha motif [SAM] and Src homology 3 [SH3] domain-containing member 3), also called SH3-containing lymphocyte protein (SLY1), is a lymphoid-specific adaptor protein encoded by an X-linked gene.[4] The SAM domain of SASH3 mediates homo- and heterodimerization, and the SH3 domain mediates protein–protein interaction by binding to proline-rich domains. SASH3 also contains 2 nuclear localization signals.[5] First identified in an adhesion assay screen using a T-cell lymphoma

complementary DNA library,[6] SASH3 was later independently identified as a protein that is phosphorylated at Ser27 following T- or B-cell receptor ligation and protein kinase C (PKC) activation.[7] However, its precise role in antigen receptor signaling is not defined. *Sly1*$^{-/-}$ and *Sly1*$^{\Delta/\Delta}$ mice,[4] the latter expressing a protein that lacks the Ser27 phosphorylation site and parts of the nuclear localization signals, are characterized by reduced lymphoid organ cellularity, impaired T-cell proliferation after CD3 and CD28 stimulation, low levels of serum immunoglobulin M (IgM) and IgG1, impaired antibody responses to T-independent and T-dependent antigens, and quantitative and qualitative defects of natural killer (NK) cells.[4,8-10] However, the role of SASH3 in human lymphoid development and function is not known.

Here, we report 4 unrelated male patients with recurrent infections, refractory autoimmune cytopenias, and profound multilineage immunodeficiency, associated with hemizygous loss-of-function *SASH3* variants. These data identify SASH3 deficiency as a novel cause of X-linked CID in humans.

Patients and methods

Study approval and study patients

Peripheral blood mononuclear cells (PBMCs) and bone marrow samples were obtained upon informed consent, according to protocols 07-I-0-033, 93-I-0119, 10-I-0014, 13-N-0017, 20-N-9962, 05-I-0213, and 17-I-0122. The study was approved by the National Institutes of Health Institutional Review Board. Table 1 provides details regarding the 4 unrelated male patients (patient 1 [P1] to P4 in Figure 1A) in this study along with histories of recurrent infections and multilineage, treatment-refractory autoimmune cytopenias. Detailed clinical information is provided in the supplemental Material (available on the *Blood* Web site).

Immune phenotyping, NK cell function, and next-generation sequencing

Peripheral blood and blood from bone marrow aspirates was processed using Ficoll (GE Healthcare, Marlborough, MA). Single-cell suspensions were stained with monoclonal antibodies directed against cell-surface molecules. Upon washing, cells were analyzed by flow cytometry using an LSR Fortessa Flow Cytometer with FACSDiva software, and the final analysis was performed using FlowJo v.10.6 software (BD Biosciences, Franklin Lakes, NJ). NK-cell degranulation in response to stimulation with K562 target cells and interleukin-12 (IL-12)/IL-18–induced NK-cell interferon γ (IFN-γ) production were tested as previously described.[11] Genomic DNA was extracted from peripheral blood and subjected to massively parallel (next-generation) sequencing on an Illumina sequencing system (San Diego, CA) (details are provided in supplemental Methods).

Plasma preparation, cell proliferation, cell cycle, and apoptosis

Plasma was prepared from heparinized blood by centrifugation at 2000*g* for 10 minutes, and levels of soluble biomarkers were measured using a V-PLEX Human Cytokine 30-Plex Kit and a SECTOR Imager 6000 Reader (both from Meso Scale Diagnostics, Gaithersburg, MD) according to the manufacturer's directions. In vitro T-cell proliferation upon stimulation with anti-CD3 and anti-CD28 (with or without IL-2), or with phosphomolybdic acid (PMA) plus ionomycin was measured by Cell Trace Violet dilution as described.[12] Cell cycle progression and apoptosis were analyzed by culturing PBMCs (5×10^5 cells per well) with either medium alone or 20 ng/mL PMA plus 500 ng/mL ionomycin or with 100 ng/mL anti-CD3 plus 100 ng/mL anti-CD28 for 72 hours. Cell cycle analysis was performed using a Click-iT EdU Alexa Fluor 647 Flow Cytometry Assay Kit (Invitrogen, Carlsbad, CA) according to the manufacturer's instructions. For apoptosis, cells were stained with a Fluorescein Isothiocyanate-Annexin V Apoptosis Detection Kit (BioLegend, San Diego, CA) and 4′,6-diamidino-2-phenylindole (DAPI) (FxCycle Violet; Invitrogen) for 30 minutes and analyzed by flow cytometry.

Western blotting and HTS of *TRA* rearrangements

Cell lysates were obtained from 1×10^6 PBMCs or from 5×10^5 T-cell enriched preparations (EasySep Human T-Cell Enrichment Kit; STEMCELL Technologies) under resting conditions or upon stimulation for 20 minutes with CD3 and CD28 (Dynabeads T-Cell Activator; Invitrogen). Samples were resolved by sodium dodecyl sulfate-polyacrylamide gel electrophoresis according to standard protocols, transferred to nitrocellulose transfer membrane (Invitrogen), and immunoblotted with specific antibodies (see supplemental Methods). Immunoreactive proteins were detected with horseradish peroxidase–coupled secondary antibodies (GE Healthcare), followed by an electrochemiluminescence assay (Thermo Fisher Scientific, Waltham, MA). PBMCs were collected and enriched for $CD3^+$ cells using the Pan T-Cell Isolation Kit (Miltenyi Biotec). High-throughput sequencing (HTS) of T-cell receptor α (*TRA*) rearrangements was performed by multiplex polymerase chain reaction, using DNA as the template (Adaptive Biotechnologies, Seattle, WA), as described.[13]

Structural modeling

Experimentally derived structures for the SH3 and SAM domains of SASH3 were combined using homology-based methods[14] and the closest experimental structures were obtained by a sequence-based search[15] of the protein data bank.[14] The SAM domain was modeled from mouse Sly1 (100% identity; 6fxf[5]). The SH3 domain was modeled from the SH3 domain of human HACS1 (92% identical; 6uzj [unpublished]). The C-terminal region of SASH3 is likely to be intrinsically disordered, using the consensus prediction from MobiDB-lite.[16] Genomic variants were assessed in their 3D context using FoldX version 4.0.[17] The effects of genomic variants on simple linear motifs were assessed using ELM[18] and custom scripts.

In vitro T-cell differentiation and correction of SASH3 deficiency

In vitro T-cell differentiation of sort-purified bone marrow–derived and mobilized peripheral blood–derived $CD34^+CD3^-$ cells was performed using the artificial thymic organoid (ATO) system, as described.[19] *SASH3*$^{-/-}$ Jurkat cells were generated using CRISPR, and their genotypes were characterized as detailed in supplemental Material. Lack of SASH3 protein expression was confirmed by western blotting. A bicistronic lentiviral vector expressing SASH3 and mCherry was generated and used to transduce *SASH3*$^{-/-}$ Jurkat cells as well as control- and patient-derived T cells, as described in supplemental Material. In parallel, cells were transduced with a mock-vector expressing mCherry only. Reconstitution of SASH3 expression was assessed by western blot. In vitro proliferation of parental *SASH3*$^{-/-}$ and gene-transduced Jurkat cells was assessed by plating the same number of cells in triplicate wells in RPMI-10% fetal bovine serum and counting the number of

Table 1. Clinical features of patients with *SASH3* mutations

	P1	P2	P3	P4
Age at first symptoms	3 y	5 y	2 y	Not known
Infections	Recurrent pulmonary infections, skin/soft tissue infections, warts	Recurrent sinopulmonary infections, *Escherichia coli* sepsis	Recurrent sinopulmonary infections, dental abscesses, sepsis, and skin infections; *Candida* esophagitis; warts	JC virus progressive multifocal leukoencephalopathy, bacterial meningitis (2 episodes), septic arthritis, sepsis, recurrent sinopulmonary infections, varicella-zoster virus, warts
Hematology	Neutropenia, chronic thrombocytopenia, T-cell large granular lymphocyte (clonal $CD8^+CD57^+$ cells) proliferation	Autoimmune hemolytic anemia, immune-mediated thrombocytopenia, autoimmune neutropenia, splenomegaly, $CD8^+CD57^+$ large granular lymphocyte T cells in bone marrow	Autoimmune hemolytic anemia, immune-mediated thrombocytopenia, autoimmune neutropenia	Immune-mediated thrombocytopenia, autoimmune hemolytic anemia, leukopenia, $CD8^+CD57^+$ large granular lymphocyte T cells in bone marrow
Neurology			Brain volume loss, seizures (end of life)	JC virus progressive multifocal leukoencephalopathy
Cardiovascular			Episodic bradycardia	
Pulmonary			Bronchiectasis, granulomatous nodules	
Endocrine		Hypothyroidism	Hypothyroidism, hypophosphatemia	
Gastrointestinal tract/liver		Hepatomegaly, suspected nodular regenerative hyperplasia	Enteropathy, nodular regenerative hyperplasia/ hepatomegaly, liver granulomas	
Skin and mucous membranes	Aphthous ulcers		Granulomatous skin lesions, aphthous ulcers	Granulomatous skin lesions

cells once per day for 4 days. Mock-transduced and SASH3-transduced control and patient-derived T cells were stimulated in vitro with anti-CD3 plus anti-CD28 for 20 minutes, as described above, and cell lysates were probed with antibodies to phosphorylated PLCγ1 (pPLCγ1), total PLCγ1, SASH3, and glyceraldehyde-3-phosphate dehydrogenase.

Statistical analysis

Differences between groups were analyzed using either the Student *t* test (for individual comparisons with Gaussian distributions), or the Mann-Whitney *U* test (for individual comparisons with non-Gaussian distributions), with statistical significance indicating a 95% confidence interval. Statistical analysis was performed using Prism (GraphPad Software, San Diego, CA).

Results

Hematologic and immunologic phenotype

At the time of genetic diagnosis, all patients were leukopenic (Table 2). Analysis of lymphocyte subsets demonstrated low $CD4^+$ T-cell counts in P1, P3, and P4 and a marked decrease of $CD4^+$ naïve T cells in all 4 patients. P2 and P4 also had low naïve $CD8^+$ T-cell counts, whereas P1 and P3 showed an elevated number of $CD8^+$ effector memory cells re-expressing CD45RA (T_{EMRA}) that expressed programmed cell death protein 1 (PD-1) and CD95 (supplemental Figure 1A). The proportion of $CD4^+CD25^{hi}CD127^{low}$ regulatory T cells (Tregs) was decreased in P1, P2, and P3 (Table 1). The distribution of T helper (T_H) cell subsets was studied by analyzing the expression of CXCR3 and CCR6 chemokine receptors on the surface of $CD4^+CD25^{low}CD45RA^-CXCR5^-$ cells.[20] Near absence of T_H1, T_H17, and T_H1* cells was observed in P1, P3, and P4, and a severe reduction of T_H17 cells was detected in P2 (supplemental Figure 1B).

All 4 patients had very low to absent $CD19^+$ B cells (Table 2). P2, P3, and P4 had previously received rituximab; however, they had been diagnosed with low IgG and IgA and defective specific antibody responses in childhood or young adulthood before receiving rituximab. P1 had profound B-cell lymphopenia and low

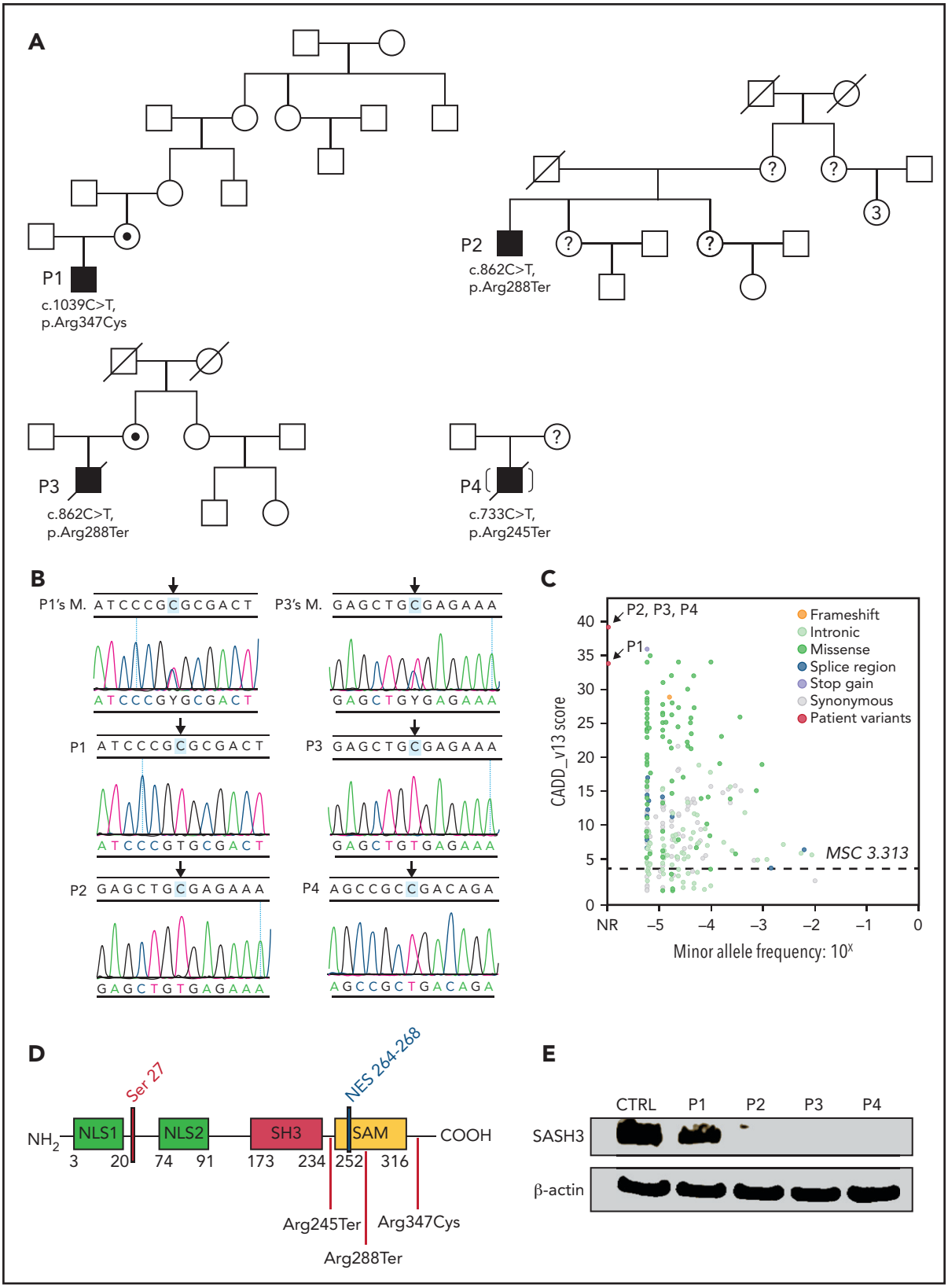

Figure 1. Pedigrees, *SASH3* genetic variants, and protein expression. (A) Pedigrees and familial segregation of mutant *SASH3* alleles. Probands are indicated as P1to P4. SASH3 variants detected by whole-exome sequencing are designated at the nucleotide and amino acid level below each patient. (B) Sanger sequencing confirmation of *SASH3* variants. The patient is identified on the upper left of each chromatogram (M., mother). Arrows designate the mutated nucleotide. Parental sequencing was not obtained for P2 or for P4 who was adopted. (C) *SASH3* variants are predicted to be damaging. Plot of combined annotation depletion dependent (CADD, version 13) score vs minor allele frequency (MAF) of *SASH3* modified from PopViz (Rockefeller University, New York, NY). The dotted horizontal line corresponds to the *SASH3* mutation significance cutoff (MSC) score. Arrows identify the CADD score of each of the SASH3 variants detected in the patients, all of which were private (MAF = 0). (D) Schematic representation of the SASH3 protein and its domains. Locations of the patients' variants are indicated by vertical red lines. Numbers indicate amino acid positions. (E) SASH3 protein is not detectable in patients with nonsense *SASH3* variants. The immunoblot shows results for SASH3 and β-actin protein expression in PBMC lysates for the patients identified above each lane. CTRL, control, NES, nuclear export signal; NLS1, nuclear localization signal 1; NLS2, nuclear localization signal 2; NR, not reported.

Table 2. Laboratory data for patients with *SASH3* mutation at the time of genetic diagnosis

	Reference range	P1	P2	P3	P4
Age at genetic diagnosis, years		19	50	27	56
SASH3 variant		p.R347C	p.R288X	p.R288X	p.R245X
White blood cell count	4.23-9.07	**2.53 (L)**	**1.89 (L)**	**2.68 (L)**	**4.11 (L)**
Hemoglobin, g/dL	13.7-17.5	15.6	**9.5 (L)**	**11.7 (L)**	15.2
Platelet count $\times 10^3/\mu L$	161-347	**156 (L)**	216	**46 (L)**	291
Absolute lymphocyte count $\times 10^3/\mu L$	1.32-3.57	1.33	**0.58 (L)**	2.01	**0.56 (L)**
Absolute neutrophil count $\times 10^3/\mu L$	1.78-5.38	**0.38 (L)**	**1.09 (L)**	**0.60 (L)**	2.74
$CD3^+$ cells per μL	714-2266	1294	**530 (L)**	2002	**339 (L)**
$CD4^+CD3^+$ cells per μL	359-1565	**140 (L)**	393	**145 (L)**	**133 (L)**
$CD4^+CD62L^+CD45RA^+CD3^+$ cells per μL	102-1041	**32 (L)**	**16 (L)**	**0 (L)**	**1 (L)**
$CD4^+CD62L^+CD45RA^-CD3^+$ cells per μL	162-614	**53 (L)**	220	**121 (L)**	**105 (L)**
$CD4^+CD62L^-CD45RA^-CD3^+$cells per μL	42-225	**20 (L)**	149	**24 (L)**	**26 (L)**
$CD4^+CD62L^-CD45RA^+CD3^+$ cells per μL	0-29	**35 (H)**	8	0	0
$CD4^+CD25^{hi}CD127^{low}$, % of $CD4^+$ cells	3-10	**2.24 (L)**	**2.27 (L)**	**0.97 (L)**	5.3
$CD8^+CD3^+$ cells per μL	178-853	**1001 (H)**	**125 (L)**	**1214 (H)**	191
$CD8^+CD62L^+CD45RA^+CD3^+$ cells per μL	85-568	181	**39 (L)**	237	**42 (L)**
$CD8^+CD62L^+CD45RA^-CD3^+$ cells per μL	25-180	37	41	28	121
$CD8^+CD62L^-CD45RA^-CD3^+$ cells per μL	24-175	52	**23 (L)**	40	**9 (L)**
$CD8^+CD62L^-CD45RA^+CD3^+$ cells per μL	11-172	**733 (H)**	21	**907 (H)**	20
$CD19^+$ cells per μL	61 -321	**4 (L)**	**13 (L)***	**0 (L)***	**8 (L)***
$CD3^-CD16^+CD56^+$ cells per μL	126-729	**33 (L)**	**36 (L)**	**0 (L)**	**124 (L)**
Serum IgG, mg/dL	700-1600	813	1425†	1364†	**173 (L)**
Serum IgA, mg/dL	70-400	82	**<5 (L)**	**<5 (L)**	**<5 (L)**
Serum IgM, mg/dL	40-230	**26 (L)**	**755 (H)**	**<5 (L)**	**<5 (L)**
Anti-pneumococcal antibody (proportion of serotypes with positive antibody titer)	Positive: >1.3 μg/mL	14/23	N/A	N/A	6/23
Anti-tetanus IgG, IU/mL	Positive: ≥0.01	0.48	N/A	N/A	0.29
Antidiphtheria IgG, IU/mL	Positive: >0.01	>1.00	N/A	N/A	0.04
Anti-*Haemophilus influenzae* IgG, mg/L	Positive: ≥1.0	1.79	N/A	N/A	ND
Anti-rubella IgG, IU/mL	Positive: >10	2.2	N/A	N/A	ND
Anti-nuclear antibody, EU	0.0-0.9	**1.0 (H)**	**1.5 (H)**	0.0	ND
Anti-thyroid peroxidase IgG, IU/mL	0.0-34.9	Negative	**73.4 (H)**	**40.7 (H)**	ND
Epstein-Barr viremia, $\log_{10}$ IU/mL		<2.07 log	Negative	Negative	Negative
Cytomegalovirus viremia, $\log_{10}$ IU/mL		Negative	Negative	Negative	Negative

Abnormal values are in bold.
EU, ELISA units; H, high; L, low; N/A, not available; ND, not done.
*Patients who had received rituximab.
†Patients who had received immunoglobulin replacement therapy.

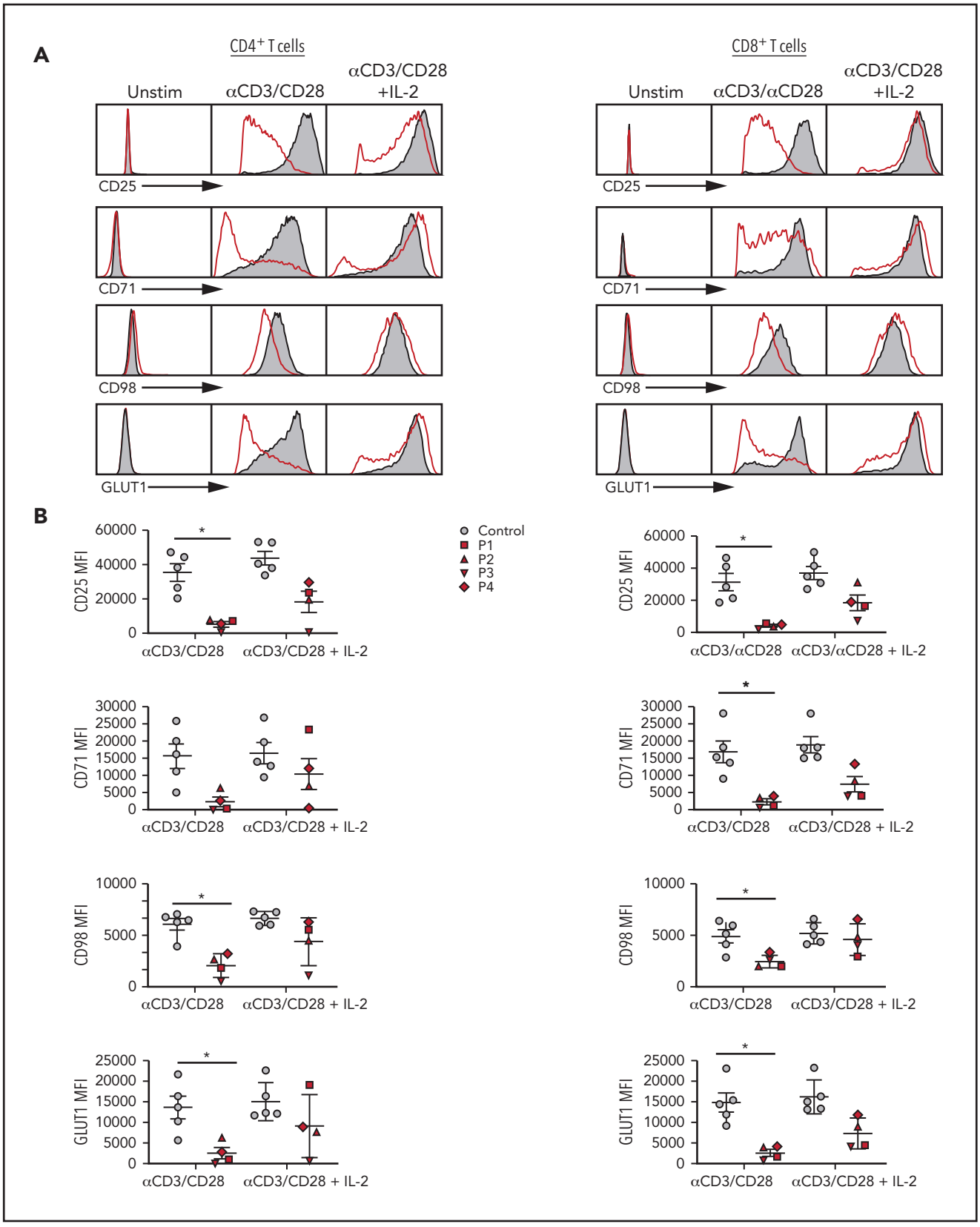

Figure 2. Activation profiles of *SASH3*-mutated T cells after in vitro stimulation with mitogens. (A) Representative plots of CD25, CD71, CD98, and GLUT1 expression in (left) $CD4^+$ and (right) $CD8^+$ T cells from P2 (red) and a healthy control (solid gray) in resting conditions or upon activation with anti-CD3 and anti-CD28 or anti-CD3 and anti-CD28 plus IL-2 in $CD4^+$ T cells. (B) Cumulative mean fluorescence intensity (MFI) data for CD25, CD71, CD98, and GLUT1 expression in (left) $CD4^+$ and (right) $CD8^+$ T cells from controls (n = 5; solid gray) and *SASH3*-mutated patients (red). Bars represent mean values ± standard error of the mean. *$P \leq .05$. Unstim, unstimulated.

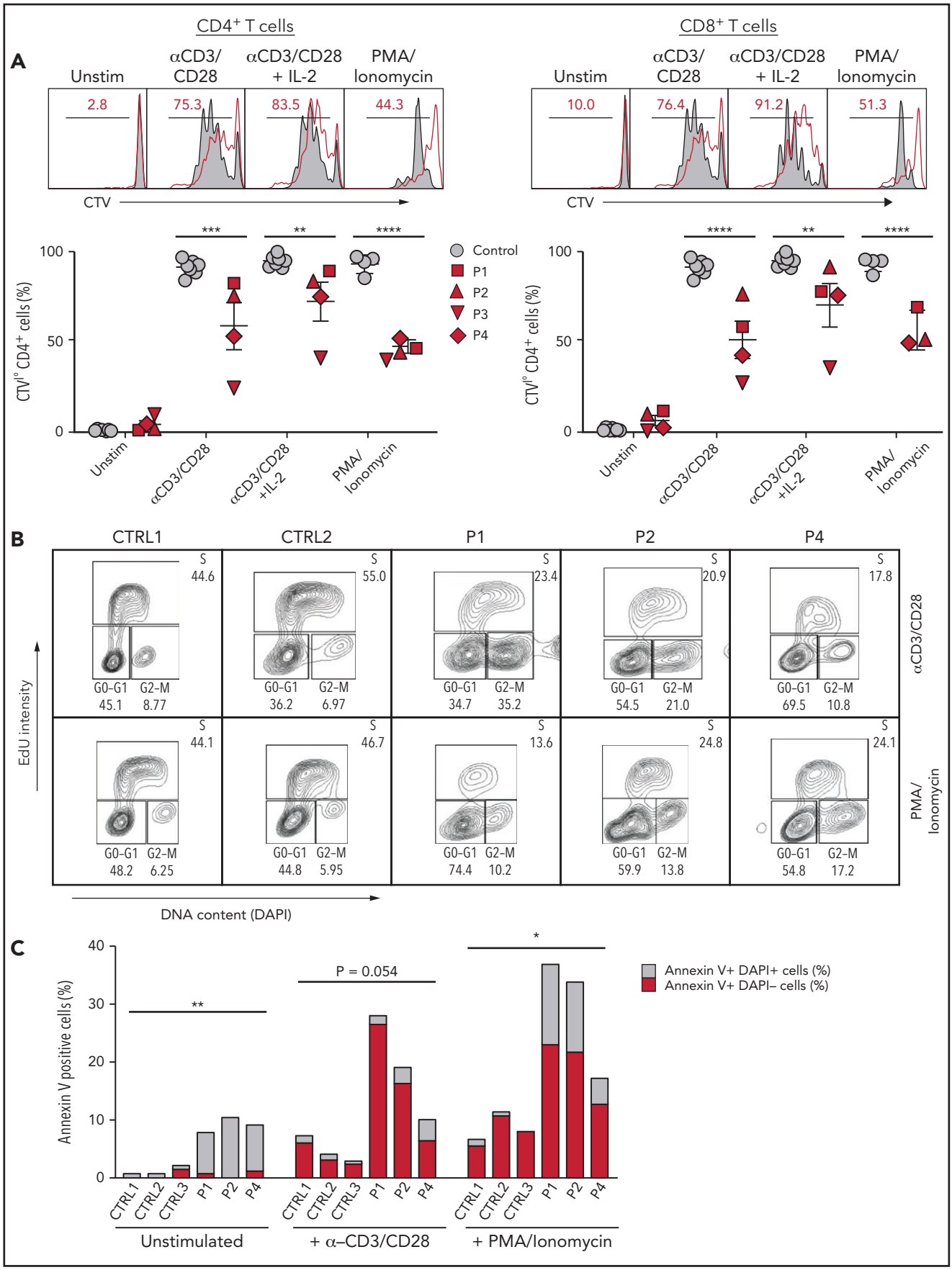

Figure 3.

serum IgM but normal IgG levels and preserved antibody responses (Table 2). Bone marrow examination was performed in P1, P2, and P4, and it revealed mild hypocellularity in P2, extensive infiltrates of $CD3^+CD8^+CD57^+$ cells in all 3 patients (supplemental Figure 2A-D), and significant expansion of $CD19^+CD20^-CD10^-CD38^{++}$ plasmablasts in P1 and P2 (supplemental Figure 3).

All patients had severe NK-cell lymphopenia (Table 1), with decreased expression of CD57, CXCR1, and KIR and increased expression of NKG2A in P1 and P2 compared with controls (supplemental Figure 4A). In vitro studies of NK-cell function were performed in P2, and they showed decreased IFN-γ expression after stimulation with IL-12 and IL-18 (supplemental Figure 4B) but normal degranulation upon coculture with K562 target cells and IL-2 (supplemental Figure 4C). Three patients had neutropenia. Increased plasma levels of several biomarkers (IL-1β, IL-6, tumor necrosis factor α, CXCL10, CCL3, CCL4, and IL-18) were documented in P1, P2, and P3, consistent with a hyperinflammatory state associated with immune dysregulation in these patients (supplemental Figure 5).

Molecular identification and characterization of *SASH3* gene defect

To search for possible underlying gene defects, we used whole-exome sequencing. No variants in genes known to be associated with inborn errors of immunity were detected. However, all 4 patients carried variants in the *SASH3* gene located on chromosome Xq26.1 (Figure 1A). In particular, P1 was hemizygous for the c.1039C>T missense variant, predicted to result in p.Arg347Cys amino acid change. The remaining 3 patients (P2, P3, and P4) were hemizygous for nonsense variants. P2 and P3 shared the same c.862C>T variant, predicted to cause an early termination at codon 288 (p.Arg288Ter). P4 was hemizygous for a c.733C>T variant (p.Arg245Ter). These variants were confirmed by Sanger sequencing, and heterozygosity for the respective variants was documented in the mothers of patients P1 and P3 (Figure 1B). None of these variants are reported in the Genome Aggregation Database (gnomAD),[21] and their combined annotation–dependent depletion (CADD) score (34 for p.Arg347Cys and 39 for both p.Arg288Ter and p.Arg245Ter) is significantly higher than the *SASH3* mutation significance cutoff (MSC) score[22] of 3.313 (Figure 1C).

The *SASH3* variants identified in P2, P3, and P4 are predicted to result in protein truncation within (P2, P3) or immediately upstream from the SAM domain (P4), whereas the missense variant detected in P1 (p.Arg347Cys) is located in the C terminus of the protein (Figure 1D). Western blotting analysis performed on PBMC lysates obtained from patients and controls with a polyclonal antibody targeting the N terminus of the SASH3 protein showed the presence of a normal-sized product in P1 at slightly reduced levels compared with control. In contrast, no SASH3 expression was detected in P2, P3, or P4 (Figure 1E), presumably as a result of nonsense-mediated RNA decay.

To facilitate interpretation of the genomic variants observed in patients, we generated a 3D model for the region of SASH3 from the beginning of the SH3 domain, through the C terminus (supplemental Figure 6). The linker between SH3 and SAM and the C-terminal region are likely highly dynamic. Although we failed to detect expression of SASH3 protein in cell lysates from P2 and P3, the p.Arg288Ter variant occurs in the second-to-last exon, leaving potential for some of the message to escape nonsense-mediated decay. Nonetheless, this variant causes partial loss of the SAM domain and disrupts the 3D structure of the domain and thereby its ability to bind other proteins. In addition, there are multiple posttranslational modifications in the C terminus that would not be present in the truncated protein. We further analyzed the possible consequences of the variant identified in P1 by an enhanced annotation approach. We investigated sequence motifs present near Arg347, a highly conserved residue from *Xenopus* through humans and identified a putative protein kinase A–binding motif. The p.Arg347Cys substitution disrupts this motif (supplemental Figure 6). Furthermore, the wild-type SASH3 protein has been measured to be phosphorylated at residue Ser349 by multiple mass spectrometry studies,[23] which supports the functional role of the motif. Thus, the p.Arg347Cys amino acid substitution may alter SASH3 activity through loss of the Ser349 regulatory phosphorylation mark.

Defective activation, proliferation, and cell cycle progression of *SASH3*-mutated T cells

Upon stimulation with anti-CD3 and anti-CD28, both $CD4^+$ and $CD8^+$ T cells from SASH3-deficient patients demonstrated impaired expression of CD25 along with CD71, CD98, and GLUT1, 3 activation-dependent metabolite transporters[24] (Figure 2A-B). These defects were associated with reduced cell proliferation (Figure 3A). The addition of exogenous IL-2 partially rescued the phenotype (Figures 2A and 3A-B). In vitro T-cell proliferation was also impaired in response to stimulation with PMA and ionomycin (Figure 3A), suggesting that distal intracellular signaling is also affected. Upon stimulation with PMA, ionomycin, anti-CD3, and anti-CD28 for 72 hours, cell cycle analysis showed that the proportion of lymphocytes in S phase and in G_2/M phase were reduced and increased, respectively, in patients compared with controls (Figure 3B). Significantly elevated proportions of early- (annexin V^+DAPI^-) and late- (annexin V^+DAPI^+) stage apoptotic cells were observed in SASH3-deficient patients under unstimulated conditions and upon stimulation with anti-CD3 and anti-CD28 or with PMA and ionomycin (Figure 3C), indicating that

Figure 3. Proliferation, cell cycle, and apoptosis of *SASH3*-mutated T cells after in vitro stimulation with mitogens. (A) Top: Representative plots showing Cell Trace Violet (CTV) staining in $CD4^+$ or $CD8^+$ T cells from P2 (red line) and control (solid gray). Red numbers correspond to the frequency of CTV^{low} proliferating cells (black bar). Bottom: Cumulative percentage of CTV^{low} cells among $CD4^+$ or $CD8^+$ T cells from controls (solid gray) or *SASH3*-mutated patients (red) in resting conditions or upon stimulation with anti-CD3 and anti-CD28, anti-CD3 and anti-CD28 plus IL-2, or PMA and ionomycin. Response to PMA and ionomycin was not studied in P3 because of a lack of available cells. Bars represent mean values ± standard error of the mean. (B) Cell cycle analysis. PBMCs from controls (CTRL1 and CRTL2) and patients (P1, P2, P4) were stimulated with anti-CD3 and anti-CD28 for 96 hours, or with PMA and ionomycin for 72 hours and then stained with 5-ethynyl-2′-deoxyuridine (EdU) and DAPI. A decreased proportion of cells in S phase and an accumulation of cells in G_2/M phase were observed in the patients. (C) Analysis of cell apoptosis. PBMCs from controls (CTRL1 to CTRL3) and patients (P1, P2, P4) were either left unstimulated or were cultured with anti-CD3 and anti-CD28 or PMA and ionomycin for 96 hours and stained with annexin V and DAPI for 30 minutes; live cells were counted by flow cytometry. P3 was not studied because of lack of available cells. Increased apoptosis was observed in all patient samples when compared with controls. Statistical analysis was performed by comparing the percentage of annexin V^+ cells in patients vs controls. $^*P \leq .05$; $^{**}P \leq .01$; $^{***}P \leq .001$; $^{****}P \leq .0001$.

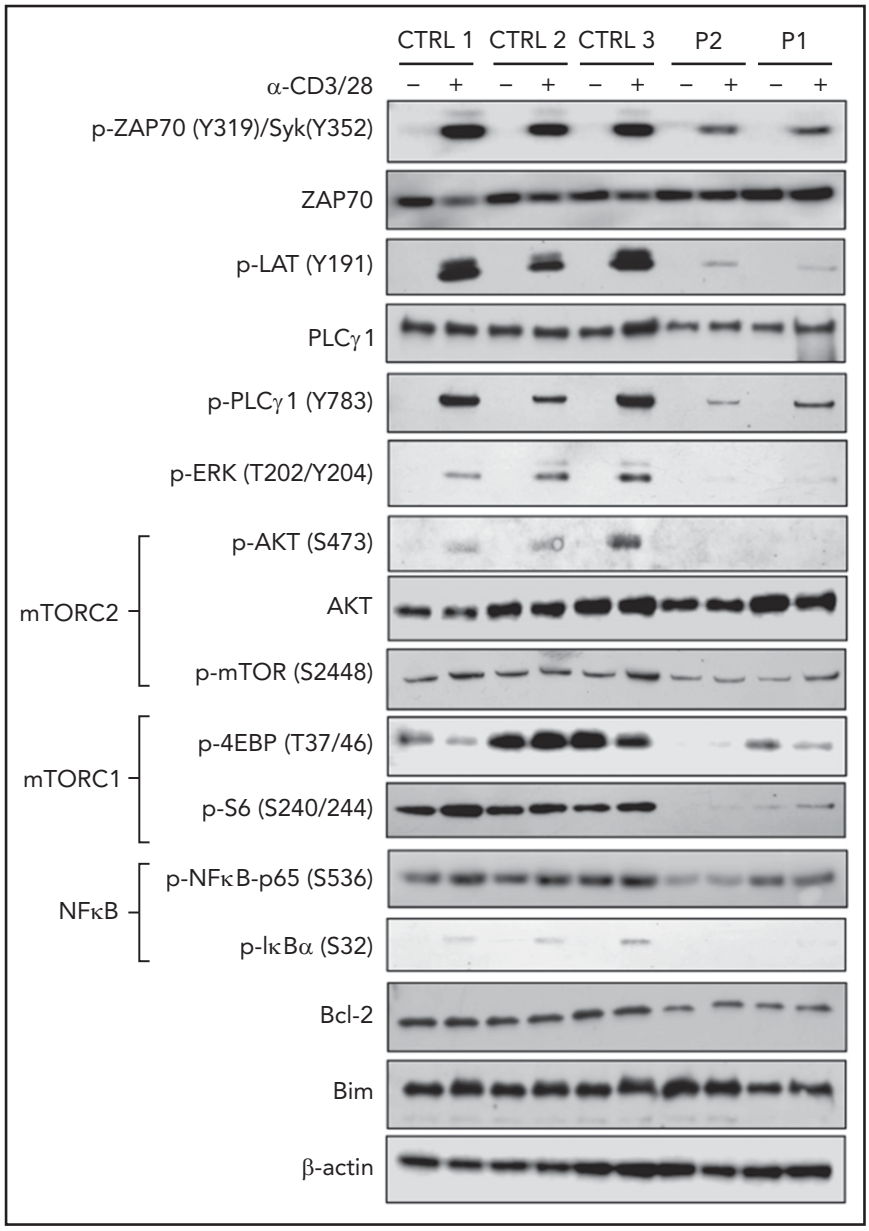

Figure 4. TCR signaling in *SASH3*-mutated patients. Immunoblots for the indicated proteins and phosphorylated proteins on lysates from 5×10^3 $CD3^+$ T cells (obtained from PBMCs upon negative selection with magnetic beads) with (+) and without (–) stimulation with anti-CD3 and anti-CD28 Dynabeads for 20 minutes from 3 healthy controls and P1 and P2. β-actin was used as loading control.

increased apoptosis may also contribute to the impaired proliferation of *SASH3*-mutated T cells.

SASH3 variants globally affect TCR signaling

To better characterize at the biochemical level how SASH3 deficiency affects T-cell receptor (TCR) signaling, we performed western blotting on T-cell lysates from P1 and P2 in resting conditions and upon stimulation with anti-CD3 and anti-CD28. A global defect of TCR signaling was detected in both patients; they had decreased levels of pZAP70, pLAT, and pPLCγ1, virtual absence of pERK and pAKT, and markedly reduced amounts of p4EBP and pS6. In addition, pIκBα was nearly absent, and levels of pNF-κB-p65 were markedly reduced. These defects were more severe in P2 than in P1, consistent with the putative hypomorphic nature of the variant in P1. Levels of the antiapoptotic protein BCL2 were decreased in patient cells (Figure 4), consistent with increased apoptosis.

Abnormalities of rearrangements at the TCRα (*TRA*) locus in patients with *SASH3* deficiency

Reduced TCR signaling may affect positive and negative selection in the thymus,[25] and impaired thymocyte survival has been reported in *Sly1*$^{-/-}$ mice.[10] To investigate whether a similar mechanism may contribute to the naïve T-cell lymphopenia observed in the patients, we analyzed composition of the *TRA* repertoire in peripheral T cells from patients and controls. During T-cell development, rearrangements at the *TRA* locus occur sequentially, so

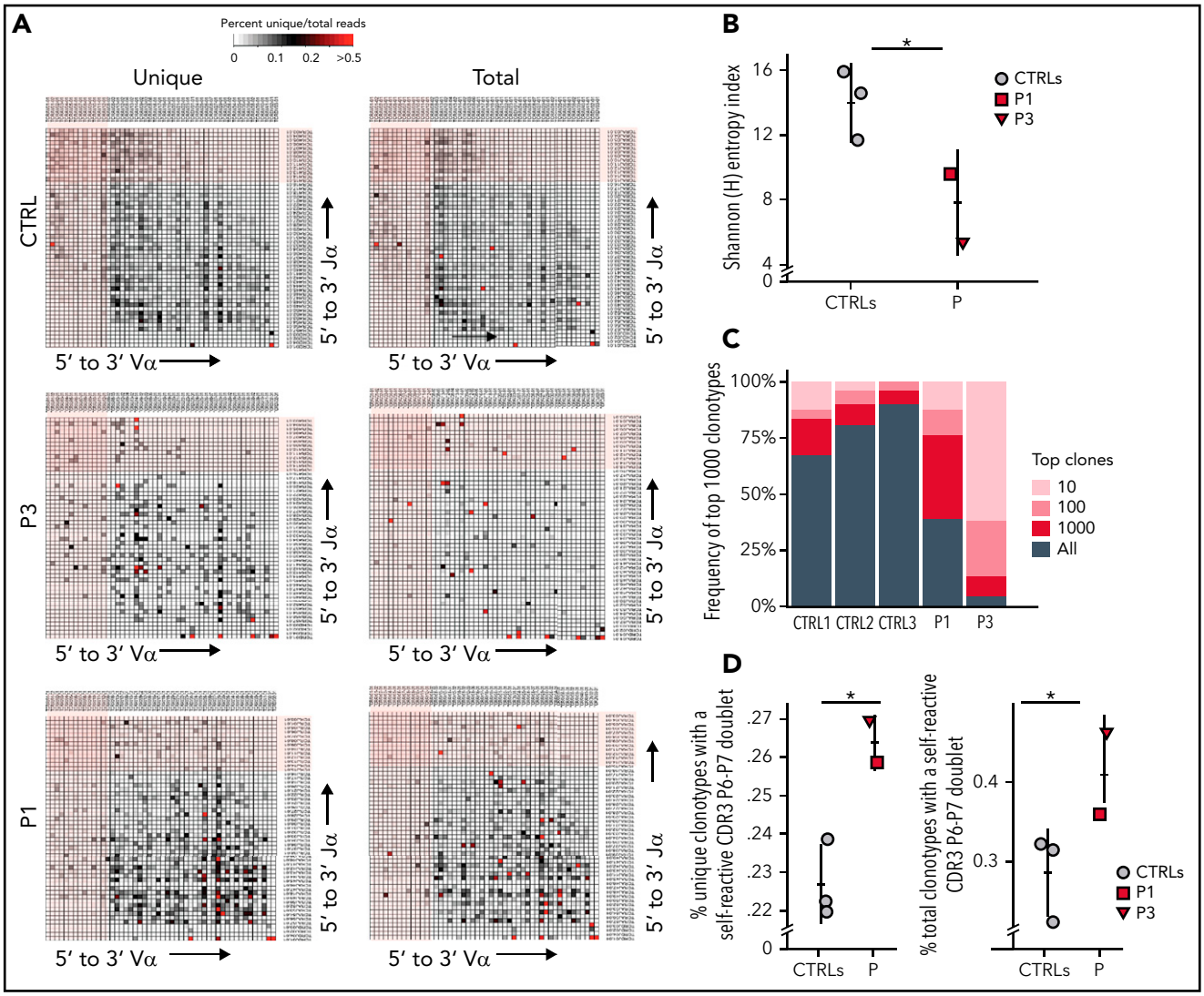

Figure 5. HTS analysis of the *TRA* repertoire in *SASH3*-mutated patients. (A) Representative heat maps depicting *Vα* and *Jα* gene pairing in (left) unique and (right) total sequences of T cells from a healthy control, P1, and P3. The most upstream *Vα* and most downstream *Jα* gene segments at the *TRA* locus are shaded in light pink. (B) Shannon [H] entropy diversity index of unique T-cell reads. (C) Representation of the frequency of 1000 most represented clonotypes among all clonotypes in T cells from 3 controls, P1, and P3. (D) Percentage of (left) unique and (right) total clonotypes containing hydrophobic amino acid residues at positions 6 and 7 (P6 and P7) of the TRA-CDR3. Results are shown for 3 healthy controls (gray circles), P1 (red square), and P3 (red triangle). Bars represent mean values ± SD (B,D). $*P < .05$.

that only thymocytes that survive long enough can rearrange the most upstream *TRAV* and the most downstream *TRAJ* genes.[26] Human genetic conditions associated with reduced thymocyte lifespan are characterized by a low number of T cells expressing Vα7.2, the product of the upstream *TRAV1/2* gene.[27,28] The proportion of $CD3^+$ cells expressing Vα7.2 (including mucosa-associated invariant T [MAIT] cells) was significantly reduced in P2, P3, and P4, whereas a normal proportion of such cells was detected in P1 (supplemental Figure 7). HTS of the *TRA* repertoire demonstrated reduced usage of the most distal *TRAV* and *TRAJ* gene segments in both unique and total sequences from P1 and P3 (Figure 5A). Moreover, decreased diversity of the T-cell repertoire (Figure 5B) and prominent clonotypic expansions (Figure 5C) were observed in both patients compared with age-matched controls. Because autoimmune cytopenia was a prominent clinical manifestation in our cohort, we analyzed the frequency of *TRA* clonotypes containing hydrophobic amino acids at positions 6 and 7 of the CDR3, a molecular biomarker of self-reactivity.[13] A higher proportion of such clonotypes was detected in both patients as compared with controls (Figure 5D). This effect was more prominent in P3 than in P1, consistent with the more severe clinical phenotype in P3.

T-cell progenitors derived from SASH3-deficient bone marrow $CD34^+$ cells display decreased survival

To further investigate whether SASH3 deficiency affects T-cell development and/or survival, we differentiated $CD34^+CD3^-$ hematopoietic stem and progenitor cells from P2 and a healthy control in the ATO system.[19] Although the $CD34^+$ cells from P2 were able to progress through various stages of T-cell differentiation, both the frequency and the absolute count of $TCR\alpha\beta^+CD3^+$ cells generated after 6 weeks of culture were significantly decreased compared with what was observed in control cells

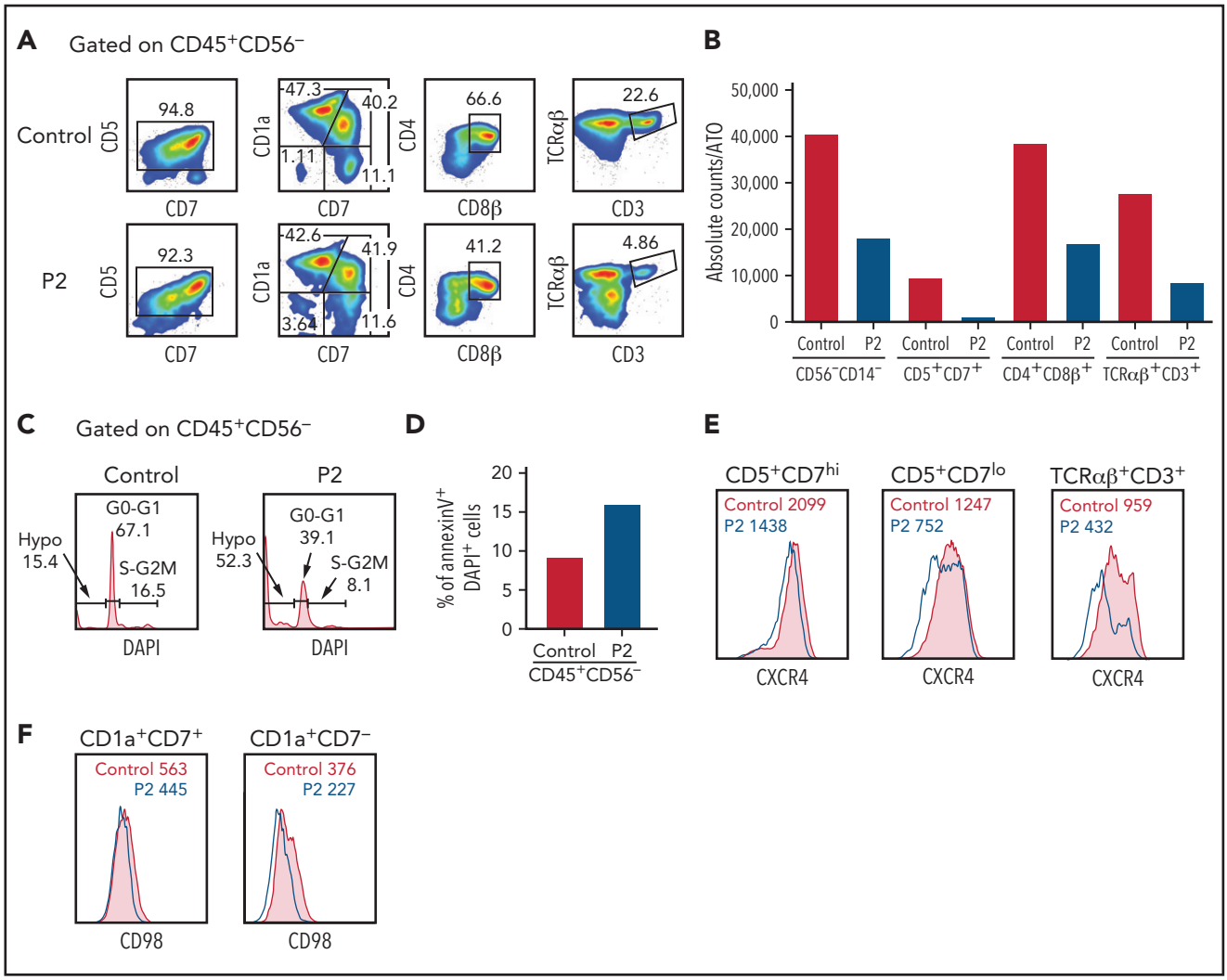

Figure 6. In vitro T-cell differentiation of CD34$^+$CD3$^-$ hematopoietic stem and progenitor cells (HSPCs). (A) Representative analysis of T-cell differentiation of control and P2 HSPCs after 6 weeks of culture in an ATO system. The fluorescence-activated cell sorter (FACS) plots show expression of early and late markers of T-cell differentiation upon gating on LIVE/DEAD$^-$CD45$^+$CD14$^-$CD56$^-$CD34$^-$ cells. (B) The bar graph shows the absolute cell counts per ATO of indicated cell subsets in control (gray bar) and P2 (red bar) samples analyzed in parallel. (C) The histograms show distribution of cells in the different phases of cell cycle after cell staining for DNA content (DAPI) in control and P2, upon gating on total CD45$^+$CD56$^-$ cells. (D) The bar graph shows the frequency of apoptotic cells after staining with annexin V and DAPI in control and P2 upon gating on total CD45$^+$CD56$^-$ cells. (E-F) FACS plot representing CXCR4 and CD98 expression in more immature (CD5$^+$CD7^{hi} or CD1a$^+$CD7$^+$) and more mature (CD5$^+$CD7^{lo} or CD1a$^+$CD7$^-$) developing T-cell progenitors and in mature TCRαβ$^+$CD3$^+$ cells.

(Figure 6A). Importantly, a reduced number of cells per ATO was also observed at earlier stages of differentiation (Figure 6B), and this defect was associated with impaired cell cycle progression and increased apoptosis, as shown by decreased frequency of cells in the S and G_2/M phases, higher frequency of hypodiploid cells (Figure 6C), and increased proportion of annexin V$^+$DAPI$^+$ late apoptotic cells (Figure 6D).

Given that CXCL12/CXCR4 signaling participates in the control of human precursor pre-TCRβ selection, cell survival, and proliferation and in the egress of mature thymocytes to the periphery,[29-31] we stained cells that differentiated in the ATO system for CXCR4 surface expression. Decreased CXCR4 expression was observed in P2 at all stages of differentiation but more prominently in more mature CD5$^+$CD7^{lo} and TCRαβ$^+$CD3$^+$ cells (Figure 6E). A similar defect in CXCR4 expression was also observed in peripheral blood T cells from P1 and P2 (supplemental Figure 8). Finally, β-selection promotes metabolic activity in developing thymocytes, including activation of the mTOR pathway and upregulation of CD98 surface expression. A slight reduction of CD98 expression was detected on the surface of differentiating CD1a$^+$CD7$^-$ cells from P2 (Figure 6F), similar to that reported in *Sly1*$^{-/-}$ and *Sly1*$^{\Delta/\Delta}$ mice.[10] Overall, in vitro T-cell differentiation data suggest that SASH3 could also play an important role in survival and activation of human thymocytes.

Rescue of SASH3 deficiency

To confirm that the abnormalities observed were a result of SASH3 deficiency, we performed rescue experiments using 2 experimental approaches. First, we generated a cellular model of SASH3 deficiency by disrupting the *SASH3* gene in Jurkat cells using CRISPR. Upon delivery of a pair of guide RNAs targeting the *SASH3* gene and subcloning in limiting dilution, a clone was identified that carried a homozygous 602nt deletion encompassing part of exon 1 and intron 1 of the *SASH3* gene (supplemental

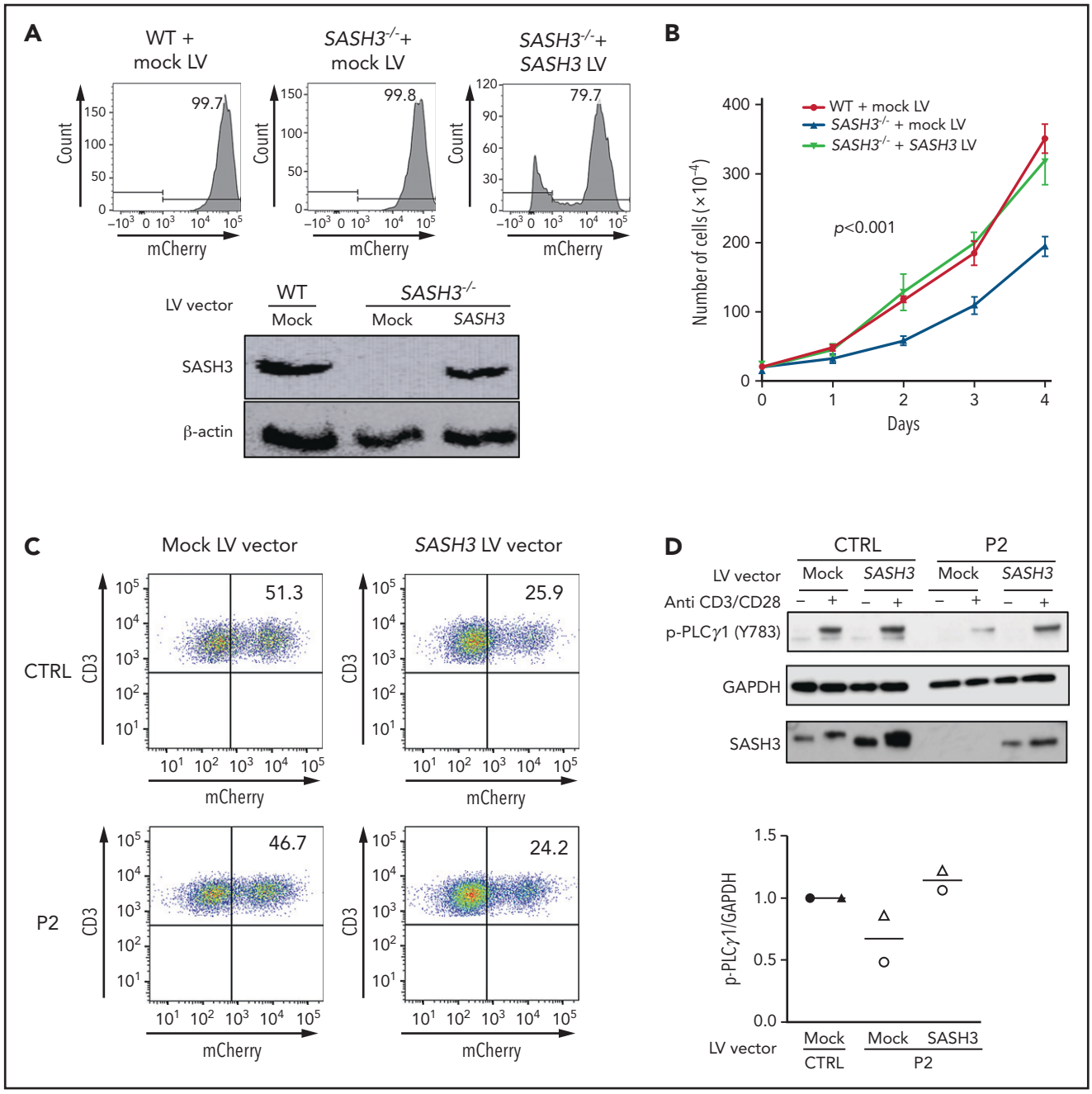

Figure 7. Lentivirus-mediated correction of SASH3 deficiency in Jurkat cells and in patient-derived T cells. (A) Top: transduction efficiency as measured by mCherry expression in wild-type (WT) and *SASH3*$^{-/-}$ Jurkat cells upon transduction with mock and *SASH3* lentivirus (LV) vectors. Bottom: western blot showing reconstitution of SASH3 protein expression in *SASH3*$^{-/-}$ Jurkat cells upon transduction with the *SASH3* LV vector. (B) Correction of the proliferative defect of *SASH3*$^{-/-}$ Jurkat cells upon transduction with the *SASH3* LV vector. WT, wild-type Jurkat; mock, *SASH3*$^{-/-}$ Jurkat cells transduced with mock LV vector; SASH3, *SASH3*$^{-/-}$ Jurkat cells transduced with the *SASH3* LV vector. Statistical significance was assessed with 2-way analysis of variance for multiple comparisons. (C) Dot-plot showing transduction efficiency (as measured by mCherry expression) in control- and P2-derived T-cell blasts upon transduction with mock and *SASH3* LV vectors. (D) Top: western blot showing reconstitution of PLCγ1 phosphorylation in *SASH3*-transduced P2 T cells upon in vitro stimulation with anti-CD3 and anti-CD28. Bottom: densitometric quantification of phosphorylated PLCγ1 (pPLCγ1) protein expression in mock- and *SASH3*-transduced P2 T cells in 2 distinct experiments (identified by different symbols). Results are expressed as pPLCγ1:glyceraldehyde-3-phosphate dehydrogenase (GAPDH) ratio and compared with what was detected in mock-transduced control cells, which were given a value of 1.0.

Figure 9A). Western blot analysis confirmed lack of SASH3 expression (supplemental Figure 9B). Compared with the parental Jurkat cell line, *SASH3*$^{-/-}$ Jurkat cells demonstrated decreased cell proliferation (supplemental Figure 9C). We then generated a bicistronic lentiviral vector that allowed expression of SASH3 and mCherry (SASH3 vector), as well as a vector that allowed expression of mCherry alone (mock vector). Transduction of the *SASH3*$^{-/-}$ Jurkat cells with the SASH3 vector rescued SASH3 expression and corrected the defect of cell proliferation to levels comparable to the parental mock-transduced Jurkat cell line (Figure 7A-B). In parallel, we used the same vectors to transduce primary T cells from a healthy control and P2. Approximately 25% of the cells were transduced with the *SASH3* vector as shown by mCherry expression (Figure 7C), yet this was sufficient to rescue PLCγ1

phosphorylation upon in vitro stimulation with anti-CD3 plus anti-CD28 (Figure 7D).

Discussion

We have described a novel X-linked inborn errors of immunity that results from SASH3 deficiency in 4 unrelated males with a history of recurrent infections and autoimmunity. The pathogenic role of the 3 *SASH3* variants identified in the patients is supported by multiple lines of evidence. In particular, none of the variants has been previously reported, and their CADD scores are significantly higher than the MSC score for the *SASH3* gene. Furthermore, the nonsense variants detected in P2, P3, and P4 are associated with loss of protein expression. The remaining missense variant detected in P1 is predicted to alter a PKA phosphorylation site and is associated with clinical and immunologic features similar to those in P2, P3, and P4. The immunologic defects identified in the patients recapitulate many of the abnormalities previously reported in *Sly1*$^{-/-}$ and *Sly1*$^{\Delta/\Delta}$ mice, including CD4^{+} T-cell lymphopenia, impaired in vitro T-cell proliferation via CD3 and CD28 (partially rescued by exogenous IL-2), decreased expression of CD71, CD98, and GLUT1 nutrient receptors, impairment of cell cycle progression, and increased T-cell apoptosis.[4,10,32]

Our data demonstrate that human SASH3 deficiency has a drastic global effect on TCR signaling, affecting phosphorylation of both proximal (ZAP-70, LAT, and PLCγ1) and distal (ERK, S6, AKT, IκBα) elements. In contrast, no defects of Akt, Erk1/2, and IκBα phosphorylation had been observed upon TCR engagement in *Sly1*$^{\Delta/\Delta}$ mice.[4] The reason for this difference remains unknown, but the profound functional T-cell defects identified in patients likely play a major role in the increased susceptibility to recurrent infections observed in the patients.

Previous studies have shown that *Sly1*$^{-/-}$ and *Sly1*$^{\Delta/\Delta}$ mice have a reduced number of double-positive and single-positive thymocytes.[10] By studying in vitro T-cell differentiation of CD34^{+} hematopoietic stem and progenitor cells, we have documented the decreased viability and the cell cycle progression of T-cell progenitors associated with generation of a reduced number of CD3^{+}TCRαβ^{+} cells in patients compared with controls. Along with skewed usage of *TRAV* and *TRAJ* genes in peripheral T cells, these data are consistent with impaired thymocyte survival in patients with SASH3 deficiency. Skewed usage of *TRAV* genes in SASH3-deficient patients was associated with severe reduction of MAIT cells. Lack of this subset has been recently reported in a patient with MR1 deficiency and persistent warts.[33] Therefore, it is possible that susceptibility to severe warts observed in SASH3-deficient patients may reflect multiple mechanisms, including impaired T-cell function, lack of MAIT cells, and NK-cell lymphopenia.

We also found that circulating T cells in patients are enriched in TCR clonotypes containing hydrophobic amino acids at the apex of CDR3, a molecular signature of self-reactive T cells.[34] We had previously shown that thymocytes with molecular signatures of self-reactivity are depleted during T-cell development in both humans and mice,[13] and an increased frequency of peripheral TCR clonotypes with molecular signatures of self-reactivity has been reported in various forms of CID with increased risk of autoimmune cytopenias.[13,35] Together, these observations suggest that SASH3 deficiency may also perturb mechanisms of negative selection in the thymus, thereby facilitating development of autoimmunity. Other immunologic abnormalities may also contribute to the high frequency of autoimmune manifestations in SASH3 deficiency, including numerical and functional Treg defects, persistence of infectious triggers, and abnormalities of B-cell function. In this regard, it is noteworthy that an expanded population of plasmablasts was detected in the bone marrow of both patients who underwent this procedure, and that 3 of the patients had a reduced proportion of circulating Tregs. P3 and P4 have been diagnosed with cutaneous and hepatic granulomas, another manifestation of immune dysregulation that has been frequently reported in patients with CID.[36-38]

NK-cell development and function are also affected by SASH3 deficiency. In particular, NK cells from *SASH3*-mutated patients were present in low numbers and showed impaired IFN-γ secretion. This observation is interesting in light of the positive correlation between SASH3 levels and IFN-γ production by human NK cells reported in a previous study.[9] A low count of NKp46^{+}CD3^{-} NK cells and impaired IFN-γ production has also been reported in *Sly1*$^{-/-}$ mice.[9] Decreased NK-cell viability was observed in mutant mice, and this defect was rescued by crossing *Sly1*$^{-/-}$ mice to *Bcl2* transgenic mice.[9] It is tempting to speculate that NK cells from SASH3-deficient patients have a survival defect, consistent with similar abnormalities observed in T cells. Rescue experiments in SASH3-deficient Jurkat cells and in patient-derived primary T cells have led to correction of the proliferation defect and of PLCγ1 phosphorylation, respectively, arguing for the causal role of SASH3 deficiency in determining the phenotype.

In summary, we have described a novel form of X-linked CID that results from SASH3 deficiency. Future studies are needed to more precisely define the role played by SASH3 in TCR signaling and NK-cell development and function, but our data demonstrate homogeneity of the clinical phenotype, with increased susceptibility to infections and treatment-refractory multilineage autoimmune cytopenias associated with immunologic abnormalities that involve all lymphoid lineages. Although this condition permits survival into adulthood, severe complications may lead to a fatal outcome. Bone marrow chimera experiments in mice have demonstrated that the immune deficiency resulting from SASH3 deficiency is hematopoietic cell-autonomous and can be corrected by bone marrow transplantation.[4] A similar option should be considered for patients with this condition.

Acknowledgments

The authors thank the patients and their families for participating in this study, and Lawrence E. Samelson and Valarie Barr for their thoughtful comments and suggestions. The authors acknowledge Elena Cho, Debbie Draper, and Meng Truong for their clinical and protocol-related support; Jia Yan, Michael Setzer, Michael Kamen, Kathleen Jevtich, Yunting Yu, Celine Hong, Leila Jamal, and Haley Hullfish of the Centralized Sequencing Initiative; Gary Fahle, Yan Su, Sujin Hwang, and Julie Niemela from the Department of Laboratory Medicine; Justin B. Lack, Vasudev Kuram, and Susan M. Huse from the National Institute of Allergy and Infectious Diseases (NIAID) Collaborative Bioinformatics Resource and the Frederick National Laboratory for Cancer Research; and Jason Barnett, Xi Cheng, Yongjie Fan, Ke Huang, Krishnaveni Kaladi, Eric Karlins, Zhiwen Li, Joseph Mackey, Andrew Oler, Daniel Veltri, Sandhya Xirasagar, Lingwen Zhang, and Satishkumar Ranganathan from the Genomic Research Integration System (GRIS), Office of Cyber Infrastructure and Computational Biology, NIAID, National Institutes of Health (NIH). The GRIS system was developed, in part, with funding from NIAID, NIH, Department of Health and Human Services, under Bioinformatics and Computational Biosciences Branch Support Services Contract HHSN316201300006W/HHSN27200002 (to MSC, Inc)

This project was supported by grants from the NIH/Division of Intramural Research, NIAID, (1 ZIA AI001222-02) (L.D.N.) and the National Cancer Institute (HHSN261200800001E).

The content of this publication does not necessarily reflect the views or policies of the US Department of Health and Human Services, nor does mention of trade names, commercial products, or organizations imply endorsement by the United States Government.

Authorship

Contribution: O.M.D., L.D.N., and P.M.M. conceived and designed experiments; O.M.D., J.R.E.B., H.S.K., M.T.Z., A.K.D., M.B., F.P., D.F., B.P., S.M., T.K., N.R.D., J.J.L., M.P., K.R.C., and J.E.N., performed the experiments; O.M.D., J.R.E.B., H.S.K., M.T.Z., A.K.D., M.B., F.P., L.D.N., B.P., S.M., N.T., S.R.D., R.G., M.B.S., J.J.L., S.M.H., J.S., D.B.K., R.U., S.D.R., and M.A.W. analyzed the data; J.R.E.B., D.H.M., I.C., L.K.D., D.V., A.A., K.M.-H., and A.F.F. provided clinical care; M.T.Z., N.T., M.P., D.B.K., R.U., S.M.H., S.D.R., P.M.M., and L.D.N. provided reagents, materials, and analysis tools; O.M.D., J.R.E.B., and L.D.N wrote the manuscript; and all authors read and approved the final manuscript.

Conflict-of-interest disclosure: The authors declare no competing financial interests.

ORCID profiles: O.M.D., 0000-0002-4772-0799; D.H.M., 0000-0001-6978-0867; M.T.Z., 0000-0001-7073-0525; A.K.D., 0000-0002-3432-3137; S.M., 0000-0002-3458-816X; B.P., 0000-0003-2499-8250; F.P., 0000-0003-4537-9061; K.R.C., 0000-0002-0771-4191; S.R.D., 0000-0002-5870-644X; J.J.L., 0000-0002-2346-8189; L.D.N., 0000-0002-8335-0262.

Correspondence: Luigi D. Notarangelo, Laboratory of Clinical Immunology and Microbiology, National Institute of Allergy and Infectious Diseases, National Institutes of Health, Building 10 CRC, Room 5-3950, MSC 1456, 10 Center Dr, Bethesda, MD 20892; e-mail: luigi.notarangelo2@nih.gov.

Footnotes

Submitted 8 November 2020; accepted 6 April 2021; prepublished online on *Blood* First Edition 19 April 2021. DOI 10.1182/blood.2020008629.

O.M.D., J.R.E.B., T.K., H.S.K., D.H.M., I.C., M.A.W., and P.M.M. contributed equally to this work.

The online version of this article contains a data supplement.

Whole-exome sequencing and T-cell receptor repertoire data have been deposited in Web-based repositories. Accession numbers are provided in the supplemental Material. Whole-exome sequencing data have been deposited in the Database of Genotypes and Phenotypes (dbGaP) for P1, P2 and P3, and in BioProject for P4. T-cell receptor repertoire data have been deposited in the Adaptive Biotechnology website (https://www.adaptivebiotech.com/). Accession numbers are provided in the supplemental Material.

REFERENCES

1. Chakraborty AK, Weiss A. Insights into the initiation of TCR signaling. *Nat Immunol.* 2014;15(9):798-807.
2. Tangye SG, Al-Herz W, Bousfiha A, et al. Human inborn errors of immunity: 2019 update on the Classification from the International Union of Immunological Societies Expert Committee. *J Clin Immunol.* 2020;40(1):24-64.
3. Speckmann C, Doerken S, Aiuti A, et al; P-CID study of the Inborn Errors Working Party of the EBMT. A prospective study on the natural history of patients with profound combined immunodeficiency: An interim analysis. *J Allergy Clin Immunol.* 2017;139(4):1302-1310.e4.
4. Beer S, Scheikl T, Reis B, Hüser N, Pfeffer K, Holzmann B. Impaired immune responses and prolonged allograft survival in Sly1 mutant mice. *Mol Cell Biol.* 2005;25(21):9646-9660.
5. Kukuk L, Dingley AJ, Granzin J, et al. Structure of the SLy1 SAM homodimer reveals a new interface for SAM domain self-association. *Sci Rep.* 2019;9(1):54.
6. Beer S, Simins AB, Schuster A, Holzmann B. Molecular cloning and characterization of a novel SH3 protein (SLY) preferentially expressed in lymphoid cells. *Biochim Biophys Acta.* 2001;1520(1):89-93.
7. Astoul E, Laurence AD, Totty N, Beer S, Alexander DR, Cantrell DA. Approaches to define antigen receptor-induced serine kinase signal transduction pathways. *J Biol Chem.* 2003;278(11):9267-9275.
8. Scheikl T, Reis B, Pfeffer K, Holzmann B, Beer S. Reduced notch activity is associated with an impaired marginal zone B cell development and function in Sly1 mutant mice. *Mol Immunol.* 2009;46(5):969-977.
9. Arefanian S, Schäll D, Chang S, et al. Deficiency of the adaptor protein SLy1 results in a natural killer cell ribosomopathy affecting tumor clearance. *OncoImmunology.* 2016;5(12):e1238543.
10. Reis B, Pfeffer K, Beer-Hammer S. The orphan adapter protein SLY1 as a novel anti-apoptotic protein required for thymocyte development. *BMC Immunol.* 2009;10(1):38.
11. Dobbs K, Tabellini G, Calzoni E, et al. Natural killer cells from patients with recombinase-activating gene and non-homologous end joining gene defects comprise a higher frequency of CD56^{bright} NKG2A^{+++} cells, and yet display increased degranulation and higher perforin content. *Front Immunol.* 2017;8:798.
12. Calzoni E, Platt CD, Keles S, et al. F-BAR domain only protein 1 (FCHO1) deficiency is a novel cause of combined immune deficiency in human subjects. *J Allergy Clin Immunol.* 2019;143(6):2317-2321.e12.
13. Daley SR, Koay HF, Dobbs K, et al. Cysteine and hydrophobic residues in CDR3 serve as distinct T-cell self-reactivity indices. *J Allergy Clin Immunol.* 2019;144(1):333-336.
14. Källberg M, Wang H, Wang S, et al. Template-based protein structure modeling using the RaptorX web server. *Nat Protoc.* 2012;7(8):1511-1522.
15. McWilliam H, Li W, Uludag M, et al. Analysis Tool Web Services from the EMBL-EBI. *Nucleic Acids Res.* 2013;41(Web Server issue):W597-W600.
16. Necci M, Piovesan D, Dosztányi Z, Tosatto SCE. MobiDB-lite: fast and highly specific consensus prediction of intrinsic disorder in proteins. *Bioinformatics.* 2017;33(9):1402-1404.
17. Schymkowitz J, Borg J, Stricher F, Nys R, Rousseau F, Serrano L. The FoldX web server: an online force field. *Nucleic Acids Res.* 2005;33(Web Server issue):W382-388.
18. Gouw M, Michael S, Sámano-Sánchez H, et al. The eukaryotic linear motif resource - 2018 update. *Nucleic Acids Res.* 2018;46(D1):D428-D434.
19. Bosticardo M, Pala F, Calzoni E, et al. Artificial thymic organoids represent a reliable tool to study T-cell differentiation in patients with severe T-cell lymphopenia. *Blood Adv.* 2020;4(12):2611-2616.
20. Ma CS, Wong N, Rao G, et al. Monogenic mutations differentially affect the quantity and quality of T follicular helper cells in patients with human primary immunodeficiencies. *J Allergy Clin Immunol.* 2015;136(4):993-1006.e1.
21. Karczewski KJ, Francioli LC, Tiao G, et al; Genome Aggregation Database Consortium. The mutational constraint spectrum quantified from variation in 141,456 humans. *Nature.* 2020;581(7809):434-443.
22. Itan Y, Shang L, Boisson B, et al. The mutation significance cutoff: gene-level thresholds for variant predictions. *Nat Methods.* 2016;13(2):109-110.
23. Hornbeck PV, Zhang B, Murray B, Kornhauser JM, Latham V, Skrzypek E. PhosphoSitePlus, 2014: mutations, PTMs and recalibrations. *Nucleic Acids Res.* 2015;43(Database issue):D512-D520.
24. Clerc I, Moussa DA, Vahlas Z, et al. Entry of glucose- and glutamine-derived carbons into the citric acid cycle supports early steps of HIV-1 infection in CD4 T cells. *Nat Metab.* 2019;1(7):717-730.
25. Melichar HJ, Ross JO, Herzmark P, Hogquist KA, Robey EA. Distinct temporal patterns of T

cell receptor signaling during positive versus negative selection in situ. *Sci Signal.* 2013; 6(297):ra92.

26. Guo J, Hawwari A, Li H, et al. Regulation of the TCRalpha repertoire by the survival window of CD4(+)CD8(+) thymocytes. *Nat Immunol.* 2002;3(5):469-476.

27. Berland A, Rosain J, Kaltenbach S, et al. PROMIDISα: A T-cell receptor α signature associated with immunodeficiencies caused by V(D)J recombination defects. *J Allergy Clin Immunol.* 2019;143(1):325-334.e2.

28. Okada S, Markle JG, Deenick EK, et al. IMMUNODEFICIENCIES. Impairment of immunity to Candida and Mycobacterium in humans with bi-allelic RORC mutations. *Science.* 2015;349(6248):606-613.

29. Trampont PC, Tosello-Trampont AC, Shen Y, et al. CXCR4 acts as a costimulator during thymic beta-selection. *Nat Immunol.* 2010; 11(2):162-170.

30. Poznansky MC, Olszak IT, Foxall R, Evans RH, Luster AD, Scadden DT. Active movement of T cells away from a chemokine. *Nat Med.* 2000;6(5):543-548.

31. Majumdar S, Murphy PM. Adaptive immunodeficiency in WHIM syndrome. *Int J Mol Sci.* 2018;20(1):3.

32. Schäll D, Schmitt F, Reis B, Brandt S, Beer-Hammer S. SLy1 regulates T-cell proliferation during Listeria monocytogenes infection in a Foxo1-dependent manner. *Eur J Immunol.* 2015;45(11):3087-3097.

33. Howson LJ, Awad W, von Borstel A, et al. Absence of mucosal-associated invariant T cells in a person with a homozygous point mutation in *MR1*. *Sci Immunol.* 2020;5(49):eabc9492.

34. Stadinski BD, Shekhar K, Gómez-Touriño I, et al. Hydrophobic CDR3 residues promote the development of self-reactive T cells. *Nat Immunol.* 2016;17(8):946-955.

35. Rowe JH, Delmonte OM, Keles S, et al. Patients with *CD3G* mutations reveal a role for human CD3γ in T_{reg} diversity and suppressive function. *Blood.* 2018;131(21): 2335-2344.

36. Leclerc-Mercier S, Moshous D, Neven B, et al. Cutaneous granulomas with primary immunodeficiency in children: a report of 17 new patients and a review of the literature. *J Eur Acad Dermatol Venereol.* 2019;33(7): 1412-1420.

37. Mathieu A-L, Verronese E, Rice GI, et al. PRKDC mutations associated with immunodeficiency, granuloma, and autoimmune regulator-dependent autoimmunity. *J Allergy Clin Immunol.* 2015;135(6):1578-1588.e5.

38. Schuetz C, Huck K, Gudowius S, et al. An immunodeficiency disease with RAG mutations and granulomas. *N Engl J Med.* 2008;358(19):2030-2038.